Strojniški vestnik - Journal of Mechanical Engineering vol(yyyy)no, p-p
DOI code

Original Scientific Paper
Received for review: yyyy-mm-dd
Received revised form: yyyy-mm-dd
Accepted for publication: yyyy-mm-dd

Control system for tensile testing device using low-cost hardware and open-source software

Matej Kranjec*, - Jernej Korinšek, - Miha Ambrož, - Robert Kunc
University of Ljubljana, Faculty of Mechanical Engineering, Chair of Modelling in Engineering Sciences and Medicine, Slovenia

The aim of the presented work is to verify whether a Raspberry Pi 3 B+ can be utilized as a low-cost device for controlling a tensile testing device used for material research purposes. A list of requirements based on the already available hardware was composed which the new controlling system had to fulfil. To connect all the necessary equipment, a connection board was constructed and some additional hardware was acquired for the system to be able to perform all the necessary tasks. The whole controlling system was also put in a small enclosure to make it portable. The controlling system software was written in C++ using the Pigpio library. The developed system was then tested and results compared to a commercially available device Instron 8802. Comparison of the results shows that the upgraded equipment can produce comparable results to commercially available devices and is sufficiently accurate to be applied for research purposes in the field of the characterization of material properties of soft tissues and other materials.
Keywords: Raspberry Pi, low-cost, tensile testing, measuring equipment.

Highlights*:*

- *Existing testing device controlling system has proven unreliable and has been upgraded.*
- *Raspberry Pi was chosen as the core of the new controlling and data acquisition system.*
- *The system was tested and compares favorably to a certified machine.*
- *The developed system is affordable to most researchers.*

0 INTRODUCTION

The everyday challenge of many researchers is to conduct experiments with a limited budget, so we strive to use as little funds as possible, but still use the equipment that is reliable enough to provide accurate and fast measurements as the protocol requires. Because of age and malfunctioning of our controlling and acquisition hardware, we wanted to upgrade that part of a specifically designed uniaxial tensile testing equipment for acquisition of soft tissue material properties in physiological conditions. The proposed system had to control a stepper motor motion and acquire data from a magnetic linear encoder and a tensile load cell.

Many researchers have already searched for a low-cost system to replace or substitute expensive devices for their research purpose and some of them chose an open source single-board computer (SBC) such as Raspberry Pi [1-26]. The main reason for using Raspberry Pi is its low cost, small size, versatility and a huge online community that can help solve problems while proposing improvements for new generations of the device. We decided to use the latest currently available version of the Raspberry Pi as the main processing unit of our tensile testing device. Because of the limitations of Raspberry Pi, a connection circuit board had to be constructed for connecting the encoder and motor controller. Also an analog to digital converter (ADC) had to be added for acquiring the data from the load cell. The goal was that the new controlling system performs at least as well as the previous system or even better. The new controlling solution was expected to be at least 80% cheaper compared to a commercially available solution on the market.

In the world of industry and research, there are many commercially available tensile testing devices from firms such as Instron [27-35], Hegewald&Peschke [36-41], TestResources [42-46], Mecmesin [47-50], Labthink [51-56] and others, where the user can buy the whole device with a controlling system included. Because we already had a tensile testing device that had been developed in our laboratory and the controlling equipment that was independent from the testing part of the machine, we were able to replace only the controlling part of the device.

Using the newly constructed controlling and data acquisition system, we want to show that the low cost equipment and simple open source software can be used for research purposes of obtaining the tensile properties of materials.

*Corr. Author's Address: Faculty of Mechanical Engineering, University of Ljubljana, Aškerčeva cesta 6, 1000 Ljubljana, Slovenia, matej.kranjec@fs.uni-lj.si

1 MATERIALS AND METHODS

1.1. Tensile testing machine hardware

The main purpose of the research is to upgrade the controlling and data acquisition part of our custom built mechanical tensile testing device (Fig. 1).

Fig 1. *Custom-made tensile testing machine for obtaining soft tissue tensile properties in physiological conditions*

The device is constructed using a standard aluminum framing system (Bosch Rexroth) [57], on which a linear ball screw drive compact module (CKK 20-145, Bosch Rexroth) [58] is mounted, driven by a stepper motor (VRDM 3913/50LWCEB, Berger Lahr) [59] through a 3:1 gear reduction gearbox (GBX080003K, Schneider electric) [60]. The motor is controlled by a motion control stepper motor drive (SD 326RU68S2, Berger Lahr) [61]. For measuring tensile loads, an S-type load cell (CTS63200KC25, AEP transducers) [62] connected to an analogue transmitter (ETA4/2IXO11D24, AEP transducers) [63] is used. Displacement of the carriage, fixed on the linear module, is measured using a magnetic linear incremental encoder system (EMIX 23, ELGO electronic) [64]. The tensile testing device in this configuration is able to produce vertical carriage speeds up to 80 mm/s and generate forces up to 2100 N, while measuring the movement with accuracy of 0.001 mm at any time.

1.2. Controlling hardware before upgrade

In the previous configuration [65], the National Instruments (NI) equipment was used for stepper motor motion control (NI PCI-7324) [66] and a NI USB module for data acquisition (NI USB-6221) [67]. The NI-Max software was used for configuration of PCI and USB cards. The experimental protocol was developed using the LabVIEW GUI software. The whole process of controlling and data acquisition was done on a personal computer (PC) running Windows XP. The sensors sampling rate for soft tissue tensile testing was set to 1 kHz.

The described system is suitable for experimental work, but only if it is properly set up in both the NI Max and LabVIEW environment. The software for motion control and data acquisition has to be properly coded by a trained person, otherwise damage to cards or controllers can occur.

1.3. Upgrade requirements

Similar as the old NI system, the newly proposed controlling and acquisition system upgrade has to:

- ensure the correct speed and distance of the motor movement in both directions,
- reliably monitor encoder movement at all times while performing any protocol that needs the measurement of distance at any motor speed and direction,
- monitor the analogue transmitter voltage and convert it to a digital signal with at least 1000 divisions of the full load cell measuring range,
- read measurement data from both the encoder and load cell with a minimum frequency of 1 kHz,
- collect all recorded data into one file or separate files that can be later combined into one,
- ensure the repeatability of measurements,
- be simple to use (error at component connection has to be impossible) and execute desired protocols (ease of use).

1.4. The hardware setup of proposed upgrade

For a cost-effective upgrade, Raspberry Pi 3 B+ (RPi) was chosen. RPi is a miniature low-cost SBC with the performance similar to a low-end desktop computer, but it has the advantage of being portable, upgradable and easily replaceable if any damage occurs. It is also

possible to integrate RPi into another system as we did. The RPi can be powered via micro USB connector using a 5 V/2.5 A power supply or via its 40-pin general purpose input output GPIO header using a 5 V input connector or even via Power over Ethernet (POE) with a POE HAT [68]. It uses a 1.4 GHz Broadcom's BCM2837B0, Cortex-A53 64-bit System on Chip (SoC) processor and 1 GB of LPDDR2 SDRAM. The connection to the RPi can be established using 2.4 GHz and 5 GHz IEEE 802.11.b/g/n/ac wireless LAN, Bluetooth 4.2/BLE or Gigabit Ethernet over USB 2.0 (max. 300 Mbps) and four USB 2.0 ports. The access to other devices is provided by an extended 40-pin GPIO header. The whole operating system is stored on a micro SD card, which is also used for measurement data storage [69]. A significant advantage of using RPi instead of another similar SBC is its widespread community, which results in timely firmware and operating system updates.

To collect tensile force data from the load cell through an analogue transmitter (load cell amplifier), an analogue to digital converter (ADC) had to be added to our system. For this purpose, a commercially available ADC board (Baart board, Efftek UK) [70] was used. The board converts the analogue signal to digital values using an 8-channel 12-bit ADC chip (MCP 3208-BI/P, Microchip Technology Inc.) [71] with a maximum sampling frequency of 100.000 samples/s. The communication with MCP 3208 is via Serial Peripheral Interface (SPI). Maximum SPI bus speed is 1 MHz and is limited by its 3.3 V power supply (the chip itself can do 2 MHz at 5.0 V). The ADC process takes 1.5 cycles to sample and 12 cycles to convert, which amounts to 13.5 µs (at 1 MHz SPI bus) per channel which can only be read one after another in a sequence. The SPI line (0 or 1) of the ADC chip on the Baart board can be selected with a jumper, enabling simultaneous connection of another Baart board to the system for possible future needs.

To connect all components of the controlling system to RPi's (GPIO) (Fig 2), a connection board was developed (Fig. 3). RPi GPIO limits safe current draw to 16 mA per pin and 50 mA distributed across all pins. The input gate threshold is approximately 1.8 V, but can range anywhere between maximum input low (0.8 V) and minimum input high (2.0 V). Output drives to high (3.3 V) or low (0 V). [72, 73].

The issues of unmatched voltage of the input signals from the magnetic encoder (5 V) and insufficient current output for motor controller (16 mA) had to be solved. For the magnetic encoder issue, a voltage divider was constructed using 4 and 6 kΩ resistors to convert the encoder 5 V signals to 3 V signals that are safe to use on RPi input GPIO pins. To amplify the signals sent to the motor controller from the RPi, an operational amplifier (MCP6002-E/P, Microchip Technology Inc.) [74] in a voltage follower configuration was mounted to the circuit board.

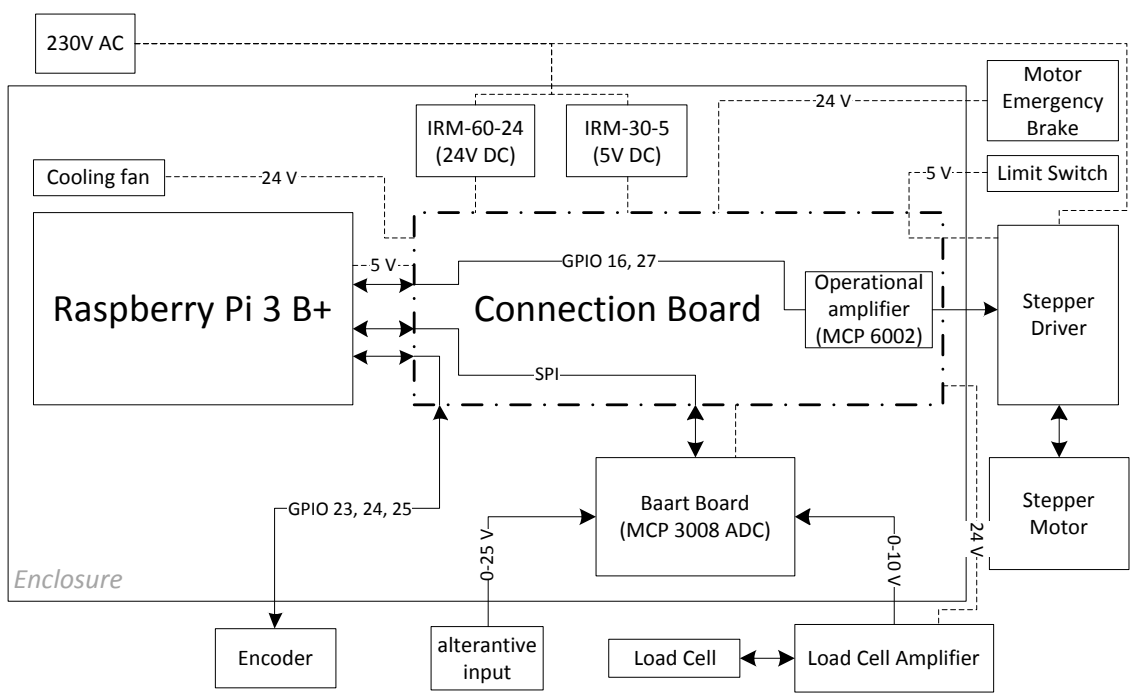

Fig 2. *Block diagram of the whole tensile testing system. Proposed upgrade is shown inside the enclosure*

The maximum output current has therefore been raised from 16 mA to 23 mA. The used operational amplifier has a 1 MHz gain bandwidth, which is fast enough for the motion controller that can receive and transmit signals with a maximum frequency of 200 kHz.

The connection board is also used to provide power to the RPi from a common 5 V power supply through a 40-pin flat ribbon cable. After initial testing, it appeared that the resistance of the flat ribbon cable wires was too high to deliver enough current at maximum operating processor load, incurring a voltage drop. For that purpose, the two 5 V power pins and at least two ground (GND) pins on the connection board had to be connected to improve the current delivery.

Fig 3. *Top view of the connection board*

Some extra wire-to-board screw terminal blocks were also added to the connection board for 5 V and 24 V DC power delivery for the motor brake, inverted motor signals (as required by the installation manual of the stepper drive [61]), operational amplifier and other future devices that need a power source which is provided using two power supplies, one for 24 V DC (IRM 60 24, Mean Well) [75] and the other for 5 V DC (IRM 30-5, Mean Well) [76]. The provided power of 60 W on the 24 V rail and 30 W on the 5 V rail is more than sufficient to fulfill the system power requirements. The detailed and complete connection scheme is available at our GitHub repository [77].

The controlling hardware enclosure was made using a short part of a wall-mounting cable raceway (Fig. 4) on which the holes were drilled for cable connectors. On one end the enclosure is covered with the front plate incorporating the power and error LED-s and the manual switch to override the limit switches. On the other end it is covered with the rear plate on which the RPi, the power switch, the power connector and a 24 V cooling fan are mounted. The plates are our own design and were manufactured in-house using a FDM 3D printer.

Fig 4. *Custom-made enclosure for the controlling hardware*

The cost of the controlling system upgrade was approximately 160 € (Table 1). In comparison to other commercially available equipment (i.e. NI modules) which can cost 1000 € or more each [78], we can easily claim that our proposed upgrade is at least 80% less costly and affordable to most researchers in the field of small-scale non-commercial tensile testing.

Table 1. *The cost of the controlling system upgrade*

Component	Quantity	Cost [€]
Raspberry Pi 3 B+	1	39.03
HDMI cable	1.5 m	4.99
micro SD card 32GB	1	16.90
multi-pin screw-in connectors	5	7.03
Custom connection PCB	1	10.60
MCP 6002 ADC IC	1	0.32
Baart board	1	20.95
IRM-30-5 PSU	1	13.62
IRM-60-24 PSU	1	15.61
Fan 24V	1	5.25
other small components	approx..	25.00
	Total:	159.30

1.5. Software setup of proposed upgrade

The operating system is based on a Raspbian Stretch Lite install (Version: April 2019, Release date: 2019-04-08) [79], using the latest testing branch repository and a Real Time kernel (4.14.y-RT) [80]. Every system service not needed for the operation has been either removed or disabled in the system software. The controlling software is run on the command line using different command arguments for every protocol implemented (Fig. 5) and the appropriate action commences.

The controlling software is written in C++ and the source code is open and available at GitHub [78]. For GPIO control the Pigpio library [82] is used. The program consists of three main functions: encoder reading, ADC reading and motor control, each running in its own thread. The functions are then interconnected. Another important part of the program is data saving and processing.

1.5.1. Encoder reading

The resolution of the magnetic encoder ELGO 23 [64] is 1 µm when four edge triggering is used. At the maximum motor speed of 95 mm/s, 95.000 pulses/s have to be sampled and processed to measure the correct distance. For this purpose, one processor thread is dedicated exclusively to acquiring signals from the encoder at all times. A call back function with four edge triggering is implemented, so every time the state of a pin changes, the function is triggered and the position is either incremented or decremented. To keep the software code simple, we did not monitor the Z signal of the encoder which is used as a 2 mm reference index and is not crucial for distance measurement.

1.5.2. Load cell reading

The load cell primary sensor is a Wheatstone bridge consisting of four resistive strain-gauges [62], which requires its signal to be amplified by a load cell amplifier [63]. The amplified signal range is between 0 and 10 V and is sampled by the ADC. An SPI reading function is implemented, which sends the appropriate bits for reading each channel and reads the result [71]. After all the required channels are read, it enters the sleep mode for a predetermined amount of time (~101 µs) repeating the cycle. Two variants of the function are implemented: one only for reading and another which signals the motor to stop if the maximal predetermined force is reached or exceeded. The latter includes an additional check whether the force reaches or exceeds this value in any three non-consecutive samples, to avoid premature signaling due to signal noise.

1.5.3. Motor control

A pulse/direction protocol is used to control the motion of the motor. For this purpose, a square wave has to be sent to the motor controller for every step of the motor. The speed of the motor is controlled by the frequency of the pulses. The shortest pulse the stepper driver can receive is 5 µs (2.5 µs up, 2.5 µs down) defining the maximum pulse frequency of 200 kHz.

Toggling the RPi GPIO outputs at those frequencies, while maintaining an equally spaced square wave, has proven difficult to be achieved consistently. To solve this problem, the built-in hardware pulse width modulation (PWM) was used because it can achieve much higher signal frequencies and is very accurate, as far as the frequency and duty cycle are concerned. This is very important for correct control of the motor speed.

Two operating modes for motor control were developed: PWM mode and Pulse mode. The PWM mode for motor control is used when accurate frequency and duty cycle is required. The Pulse mode for motor control is intended for accurate positioning.

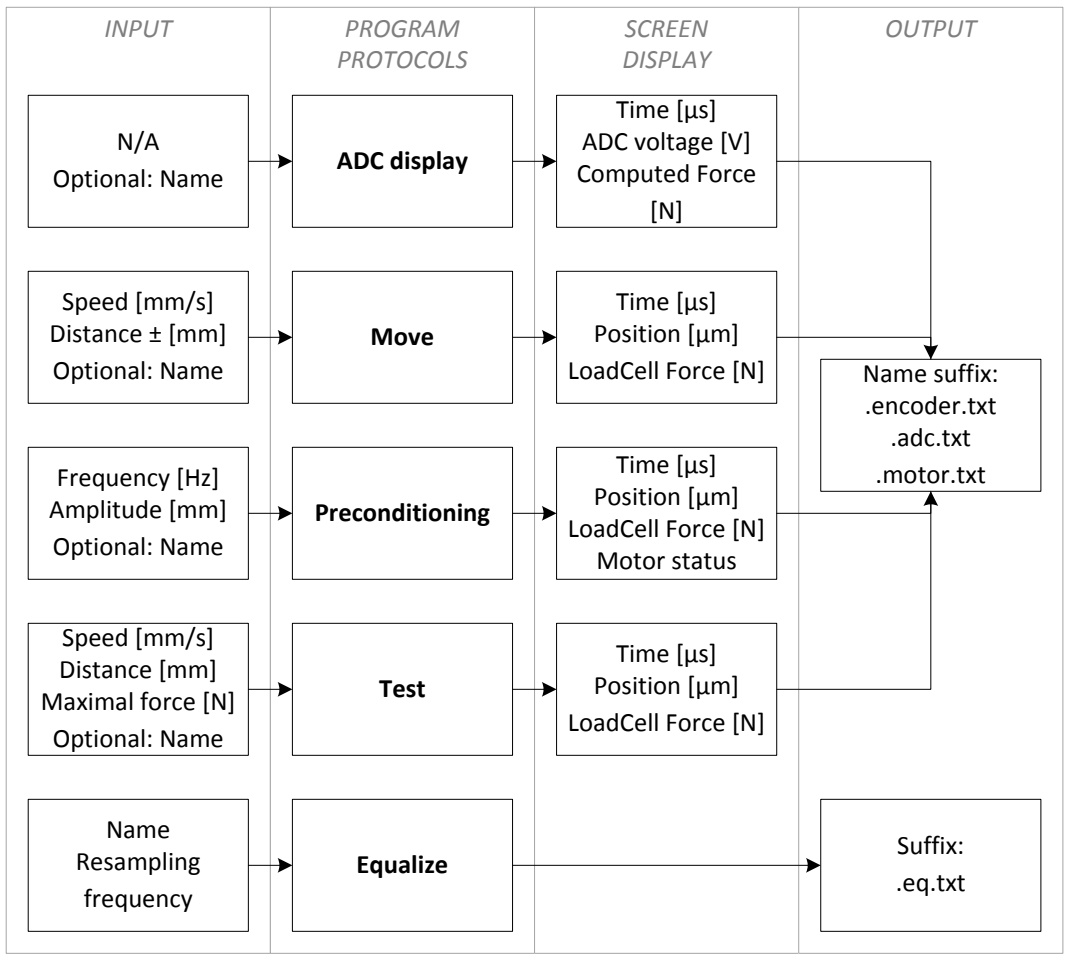

Figure 5. *Schematics of the implemented protocols*

In PWM mode, hardware PWM on RPi is used and the duration is calculated. For the duration, the sleep function is used, and the CPU is free to perform other tasks. It also takes some time to switch PWM ON and OFF. Because of this, the system can overshoot for a few pulses (<10 pulses equaling <0.01 mm on full scale or <0.01%). In Pulse mode, we generate the square wave signal in software using busy loops in between. However, the frequency and duty cycle stability of this mode are not very high as it can occasionally miss the frequency by up to 10%.

1.5.4. Data saving and processing

Because the data acquisition system runs on the RPi's Operating System (OS), the sample times are not equally spaced in time. In this configuration, the samples are approximately 250 µs apart, but the tests show that the actual interval can range from 200-300 µs. The samples from ADC, encoder and motor are also not sampled at the exact same time. To remedy this design limitation, a data processing protocol called "Equalize" was implemented.

The "Equalize" protocol takes the data from the measurement files and produces a new file suffixed by ".eq.txt" containing equally spaced time series data from all three files. This works by taking the latest available sample before each time step while discarding all the other samples in between [78]. A time step of 1000 µs proved to be a reliable choice producing stable results.

1.6. Validation of upgraded system

To validate the proposed system upgrade, tensile testing measurements were conducted on our device and on the reference device, the Instron 8802 system [82]. The protocols (Table 2) consisted of 5 loading and

unloading cycles, triangularly shaped (Fig. 6, 7 and 8), using a metal tension spring after pretensioning it to the load of 50 N.

Table 2. Validation protocol parameters

Speed [mm/s]	Distance [mm]	Frequency [Hz]
5	10	0.2500
5	50	0.0500
5	75	0.0333
10	10	0.5000
10	50	0.1000
10	75	0.0666
25	10	1.2500
25	50	0.2500
25	75	0.1666
50	10	2.5000
50	50	0.5000
50	75	0.3333

The results of all tensile tests were then compared and evaluated. Measurement of maximal speed and displacement of our device have also been conducted to determine the limits of its capabilities. The load cell used on our device had a range of 200 kg and the one on Instron 8802 had the range of 1 kN.

2 RESULTS

The results of the comparison between our device and Instron 8802 are shown in the figures 6 to 9. The left Y axis shows the tensile force from the load cell and the right axis shows the displacement of the tensile testing head measured by the linear encoder. For representation purposes, all charts (Fig. 6, 7 and 8) have the same scale on all three axes.

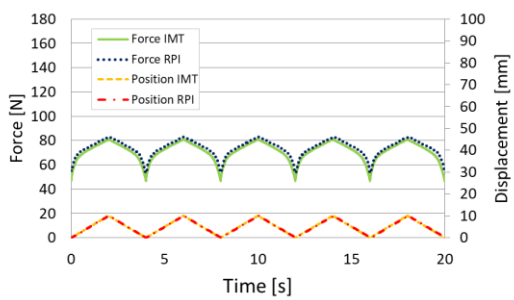

Fig. 6 *Comparison of Instron 8802 (IMT) and our device (RPi) at 10 mm distance and frequency of 0.25 Hz*

The measured force from Instron 8802 (IMT) and our device (RPi) shows a small difference of around 6 N which is constant throughout the whole protocol. The difference is a result from inaccurate pretensioning of the spring before the protocol on each device.

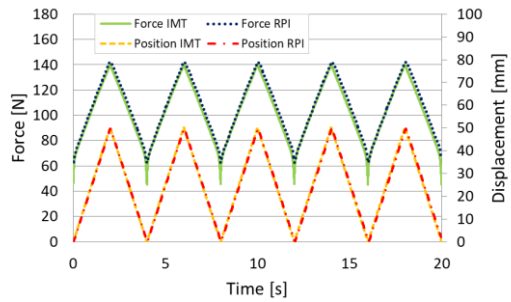

Fig. 7 *Comparison of Instron 8802 (IMT) and our device (RPi) at 50 mm distance and frequency of 0.25 Hz*

After the data acquisition the measured force from our device was filtered using a 10 Hz Low-pass filter to exclude spikes that occurred due to sampling the load cell with a greater measuring range than the one on Instron 8802 [82].

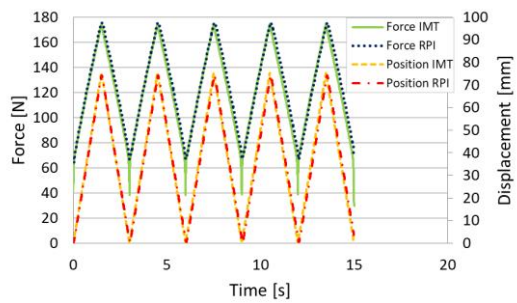

Fig. 8 *Comparison of Instron 8802 (IMT) and our device (RPi) at 75 mm distance and frequency of 0.333 Hz*

The force and displacement response difference in time is minimal, but occurs due to the "Soft-start" option on motor controller, which limits the starting acceleration of the stepper motor to reduce wear on the motor and other hardware of the tensile device. The "Soft-start" option could be turned off, resulting in much lower maximal speed of the tensile device and higher wear on the stepper motor.

All measurements also showed similar characteristics of the metal spring (Fig. 9) which also reflects in very high Pearson correlation coefficient (Table 3).

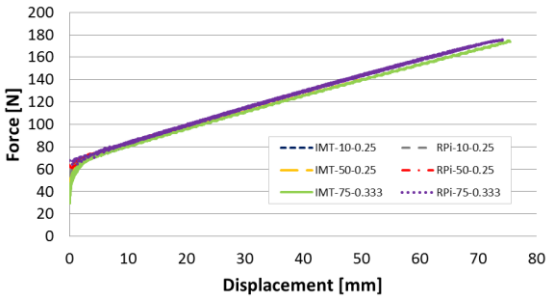

Fig. 9 *Characteristics of the metal spring at three different protocols*

Table 3. *Pearson coefficient for measurements shown in previous graphs*

	10 mm – 0.25 Hz	50 mm – 0.25 Hz	75 mm – 0.333 Hz
Pearson correlation	0.99337	0.99531	0.99018

Using the same spring, a full range tensile test was also conducted (Fig. 10) at slow speed (10 mm/s) and at the maximum device speed (95 mm/s). Both measurements show the same force-displacement response of the spring (Fig. 11).

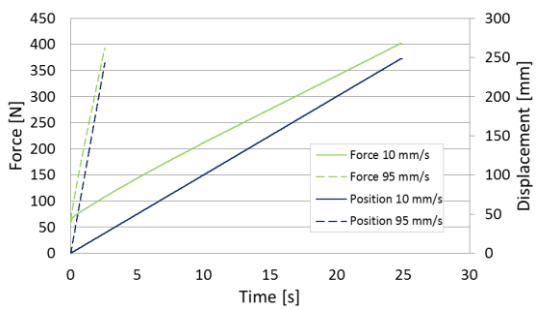

Fig. 10 *Metal spring response at 10 mm/s and 95 mm/s loading speed for a distance of 250 mm*

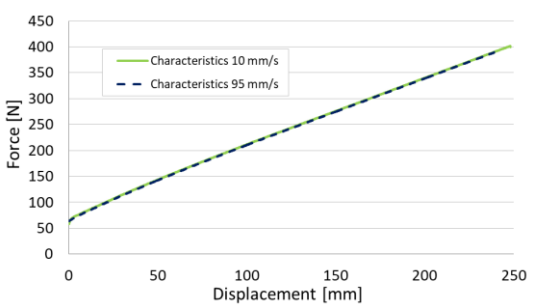

Fig. 11 *Metal spring "force-displacement" response at two different loading speeds*

3 DISCUSSION AND CONCLUSIONS

The principal purpose of the presented research and development was to test whether the principles of designing low-cost data acquisition systems can be applied to a somewhat more complex system for tensile testing. The design of the system was adopted from the existing tensile testing machine, which has proven problematic from the usability and durability point of view. The reasoning behind the component selection was to integrate a system, which will provide the same level of measurement accuracy for an affordable price. This was the reason for selecting the low-cost off-the-shelf hardware and development of own software using previously acquired experience.

The resulting system is a well-balanced compromise between invested resources and the quality of the resulting product. Using our product, we managed to control the whole tensile testing system with sufficient speed and accuracy to use it for experimental testing of soft tissues. We successfully replaced the expensive and unreliable existing controlling equipment with low-cost hardware running open source software developed in-house.

The results from the comparison of our custom-built tensile testing device with the upgraded controlling system and a commercially available certified tensile testing device Instron 8802 show that our device can produce comparable results and is sufficiently accurate to be used for research purposes. The typical dynamic tests of a steel tensile spring, conducted on both systems, yielded results with Pearson correlation over 99%.

The upgraded system is currently being used for acquiring the material properties of samples of post-mortem human ligament tissues. Although the application is currently limited to a single purpose, the controlling and data acquisition system can be easily utilized for other types of measurements or be transferred to another mechanical system.

Compared to the available turn-key solutions our system did take more time to design and develop yet it is more versatile, less costly and easily adaptable, while maintaining a comparable level of accuracy. The development of the presented system also enriched our expertise in this field, which has encouraged us to consider upgrading or developing future measurement systems in the similar manner.

4 ACKNOWLEDGMENTS

This research was funded by the Slovenian Research Agency (ARRS) as part of the Young Researcher Programme for the P2-0109 Research Programme.

5 REFERENCES

[1] Foster, S.W., Alirangues, M.J., Naese, J.A., Constans, E., Grinias, J.P. (2019). A low-cost, open-source digital stripchart recorder for chromatographic detectors using a Raspberry Pi. *Journal of Chromatography A*, vol. 1603, p. 396-400, **DOI:10.1016/j.chroma.2019.03.070**.

[2] Oltean, S.E. (2019). Mobile Robot Platform with Arduino Uno and Raspberry Pi for Autonomous Navigation. *Procedia Manufacturing*, vol. 32, p. 572-577, **DOI:10.1016/j.promfg.2019.02.254**.

[3] Khalifa, A.F., Badr, E., Elmahdy, H.N. (2019). A survey on human detection surveillance systems for Raspberry Pi. *Image and Vision Computing*, vol. 85, p. 1-13, **DOI:10.1016/j.imavis.2019.02.010**.

[4] Anandhalli, M., Baligar, V.P. (2018). A novel approach in real-time vehicle detection and tracking using Raspberry Pi. A*lexandria Engineering Journal*, vol. 57, no. 3, p. 1597-1607, **DOI:10.1016/j.aej.2017.06.008**.

[5] Kuziek, J.W.P., Shienh, A., Mathewson, K.E. (2017). Transitioning EEG experiments away from the laboratory using a Raspberry Pi 2. *Journal of Neuroscience Methods*, vol. 277, p. 75-82, **DOI:10.1016/j.jneumeth.2016.11.013**.

[6] Kirby, J., Chapman, L., Chapman, V. (2018). Assessing the Raspberry Pi as a low-cost alternative for acquisition of near infrared hemispherical digital imagery. *Agricultural and Forest Meteorology*, vol. 259, p. 232-239, **DOI:10.1016/j.agrformet.2018.05.004**.

[7] Wisnusenna, S., Yonatan, M.S., Wibisurya, A., Fanny, T., Yuwono, T. (2018). Model of Web Based Application to Control Bridge Traveler Using Raspberry Pi. *Procedia Computer Science*, vol. 135, p. 518-525, **DOI:10.1016/j.procs.2018.08.204**.

[8] Machangpa, J.W., Chingtham, T.S. (2018). Head Gesture Controlled Wheelchair for Quadriplegic Patients. *Procedia Computer Science*, vol. 132, p. 342-351, **DOI:10.1016/j.procs.2018.05.189**.

[9] Arumuga Perumal, V.S., Baskaran, K, Rai, S.K. (2017). Implementation of effective and low-cost Building Monitoring System(BMS) using raspberry PI. *Energy Procedia*, vol. 143, p. 179-185, **DOI:10.1016/j.egypro.2017.12.668**.

[10] Shah, D., Haradi, V. (2016). IoT Based Biometrics Implementation on Raspberry Pi. *Procedia Computer Science*, vol. 79, p. 328-336, **DOI:10.1016/j.procs.2016.03.043**.

[11] Pasquali, V., D'Alessandro, G., Gualtieri, R., Leccese, F. (2017). A new data logger based on Raspberry-Pi for Arctic Notostraca locomotion investigations. *Measurement*, vol. 110, p. 249-256, **DOI:10.1016/j.measurement.2017.07.004**.

[12] Žáková, K., Rábek, M. (2018). Remote Control of Thermo-opto-mechanical Plant via Raspberry Pi. *IFAC-PapersOnLine*, vol. 51, no. 6, p. 479-483, **DOI:10.1016/j.ifacol.2018.07.188**.

[13] Vujović, V., Maksimović, M. (2015) Raspberry Pi as a Sensor Web node for home automation. *Computers & Electrical Engineering*, vol. 44, 2015, p. 153-171, **DOI:10.1016/j.compeleceng.2015.01.019**.

[14] Pereira, R.I.S., Dupont, I.M., Carvalho, P.C.M., Jucá, S.C.S. (2018). IoT embedded linux system based on Raspberry Pi applied to real-time cloud monitoring of a decentralized photovoltaic plant. *Measurement*, vol. 114, p. 286-297, **DOI:10.1016/j.measurement.2017.09.033**.

[15] Ambrož, M. (2017). Raspberry Pi as a low-cost data acquisition system for human powered vehicles. *Measurement*, vol. 100, p. 7-18, **DOI:10.1016/j.measurement.2016.12.037**.

[16] Dudas, R., VandenBussche, C., Baras, A., Ali, S.Z., Olson, M.T. (2014). Inexpensive telecytology solutions that use the Raspberry Pi and the iPhone. *Journal of the American Society of Cytopathology*, vol. 3, no. 1, p. 49-55, **DOI:10.1016/j.jasc.2013.09.005**.

[17] Noorshams, O., Boyd, J.D., Murphy, T.H. (2017). Automating mouse weighing in group homecages with Raspberry Pi micro-computers. *Journal of Neuroscience Methods*, vol. 285, p. 1-5, **DOI:10.1016/j.jneumeth.2017.05.002**.

[18] Kassis, T., Perez, P.M., Yang, C.J.W., Soenksen, L.R., Trumper, D.L., Griffith, L.G. (2019). PiFlow: A biocompatible low-cost programmable dynamic flow pumping system utilizing a Raspberry Pi Zero and commercial piezoelectric pumps. *HardwareX*, vol. 4, e00034, **DOI:10.1016/j.ohx.2018.e00034**.

[19] Bolaños, F., LeDue, J.M., Murphy, T.H. (2017). Cost effective raspberry pi-based radio frequency identification tagging of mice suitable for automated in vivo imaging. *Journal of*

Neuroscience Methods, vol. 276, p. 79-83, **DOI:10.1016/j.jneumeth.2016.11.011**.

[20] Tomar, V.S., Bhatia, V. (2015). Low Cost and Power Software Defined Radio Using Raspberry Pi for Disaster Effected Regions. *Procedia Computer Science*, vol. 58, p. 401-407, **DOI:10.1016/j.procs.2015.08.047**.

[21] Lewis, A.J., Campbell, M., Stavroulakis, P. (2016). Performance evaluation of a cheap, open source, digital environmental monitor based on the Raspberry Pi. *Measurement*, vol. 87, p. 228-235, **DOI:10.1016/j.measurement.2016.03.023**.

[22] Stradolini, F., Tuoheti, A., Kilic, T., Demarchi, D., Carrara, S. (2018). Raspberry-Pi based system for propofol monitoring. *Integration*, vol. 63, p. 213-219, **DOI:10.1016/j.vlsi.2018.04.004**.

[23] Schmidt, M., Penner, D., Burkl, A., Stojanovic, R., Schümann, T., Beckerle, P. (2016). Implementation and evaluation of a low-cost and compact electrodermal activity measurement system. *Measurement*, vol. 92, p. 96-102, **DOI:10.1016/j.measurement.2016.06.007**.

[24] Andria, G., Attivissimo, F., Di Nisio, A., Lanzolla, A.M.L., Pellegrino, A. (2016). Development of an automotive data acquisition platform for analysis of driving behavior. *Measurement*, vol. 93, p. 278-287, **DOI:10.1016/j.measurement.2016.07.035**.

[25] Fletcher, J., Malalasekera, W. (2016). Development of a user-friendly, low-cost home energy monitoring and recording system. *Energy*, vol. 111, p. 32-46, **DOI:10.1016/j.energy.2016.05.027**.

[26] Tivnan, M., Gurjar, R., Wolf, D.E., Vishwanath, K. (2015). High Frequency Sampling of TTL Pulses on a Raspberry Pi for Diffuse Correlation Spectroscopy Applications. *Sensors*, vol. 15, p. 19709-19722, **DOI:10.3390/s150819709**.

[27] Smeets, K., Bellemans, J., Scheys, L., Eijnde, B.O., Slane, J., Claes, S. (2017). Mechanical Analysis of Extra-Articular Knee Ligaments. Part two: Tendon grafts used for knee ligament reconstruction. *The Knee*, vol. 24, no. 5, p. 957-964, **DOI:10.1016/j.knee.2017.07.011**.

[28] Smeets, K., Slane, J., Scheys, L., Claes, S., Bellemans, J. (2017). Mechanical Analysis of Extra-Articular Knee Ligaments. Part One: Native knee ligaments. *The Knee*, vol. 24, no. 5, p. 949-956, **DOI:10.1016/j.knee.2017.07.013**.

[29] Chandrashekar, N., Hashemi, J., Slauterbeck, J., Beynnon, B.D. (2008). Low-load behaviour of the patellar tendon graft and its relevance to the biomechanics of the reconstructed knee. *Clinical Biomechanics*, vol. 23, no. 7, p. 918-925, **DOI:10.1016/j.clinbiomech.2008.03.070**.

[30] Sivakumar, D., Ng, L.F., Zalani, N.F.M., Selamat, M.Z., Ab Ghani, A.F., Fadzullah, S.H.S.M. (2018). Influence of kenaf fabric on the tensile performance of environmentally sustainable fibre metal laminates. *Alexandria Engineering Journal*, vol. 57, no. 4, p. 4003-4008, **DOI:10.1016/j.aej.2018.02.010**.

[31] Gaaz, T.S., Luaibi, H.M., Al-Amiery, A.A., Kadhum, A.A.H. (2018). Effect of phosphoric acid on the morphology and tensile properties of halloysite-polyurethane composites. *Results in Physics*, vol. 9, p. 33-38, **DOI:10.1016/j.rinp.2018.02.008**.

[32] Gebisa, A.W., Lemu, H.G. (2019). Influence of 3D Printing FDM Process Parameters on Tensile Property of ULTEM 9085. *Procedia Manufacturing*, vol. 30, p. 331-338, **DOI:10.1016/j.promfg.2019.02.047**.

[33] Király, M., Antók, D.M., Horváth, L., Hózer, Z. (2018). Evaluation of axial and tangential ultimate tensile strength of zirconium cladding tubes. *Nuclear Engineering and Technology*, vol. 50, no. 3, p. 425-431, **DOI:10.1016/j.net.2018.01.002**.

[34] Simonovski, I., Baraldi, D., Holmström, S., Altstadt, E., Delville, R., Bruchhausen, M. (2018). Determining the ultimate tensile strength of fuel cladding tubes by small punch testing. *Journal of Nuclear Materials*, vol. 509, p. 620-630, **DOI:10.1016/j.jnucmat.2018.07.041**.

[35] Yang, Y., Li, L., Zhao, J. (2019). Mechanical property modeling of photosensitive liquid resin in stereolithography additive manufacturing: Bridging degree of cure with tensile strength and hardness. *Materials & Design*, vol. 162, p. 418-428, **DOI:10.1016/j.matdes.2018.12.009**.

[36] Zhong, S., Baitalow, F., Reinmöller, M., Meyer, B. (2019). Relationship between the tensile strength of irregularly shaped coal particles and various fuel properties. *Fuel*, vol. 236, p. 92-99, **DOI:10.1016/j.fuel.2018.08.140**.

[37] Löffl, C., Saage, H., Göken, M. (2019). In situ X-ray tomography investigation of the crack formation in an intermetallic beta-stabilized TiAl-alloy during a stepwise tensile loading. *International Journal of Fatigue,* vol. 124, p. 138-148, **DOI:10.1016/j.ijfatigue.2019.02.035**.

[38] Kuhn, P., Catalanotti, G., Xavier, J., Ploeckl, M., Koerber, H. (2018). Determination of the crack resistance curve for intralaminar fiber tensile failure mode in polymer composites under high

rate loading. *Composite Structures*, vol. 204, p. 276-287, **DOI:10.1016/j.compstruct.2018.07.039**.

[39] Yvell, K., Grehk, T.M., Hedström, P., Borgenstam, A., Engberg, G. (2018). EBSD analysis of surface and bulk microstructure evolution during interrupted tensile testing of a Fe-19Cr-12Ni alloy. *Materials Characterization*, vol. 141, p. 8-18, **DOI:10.1016/j.matchar.2018.04.035**.

[40] Yvell, K., Grehk, T.M., Hedström, P., Borgenstam, A., Engberg, G. (2018). Microstructure development in a high-nickel austenitic stainless steel using EBSD during in situ tensile deformation. *Materials Characterization*, vol. 135, p. 228-237, **DOI:10.1016/j.matchar.2017.11.046**.

[41] Margossian, A., Bel, S., Hinterhoelzl, R. (2016). On the characterisation of transverse tensile properties of molten unidirectional thermoplastic composite tapes for thermoforming simulations. *Composites Part A: Applied Science and Manufacturing*, vol. 88, p. 48-58, **DOI:10.1016/j.compositesa.2016.05.019**.

[42] Kim, W., Argento, A., Flanigan, C., Mielewski, D.F. (2015). Effects of soy-based oils on the tensile behavior of EPDM rubber. *Polymer Testing*, vol. 46, p. 33-40, **DOI:10.1016/j.polymertesting.2015.06.015**.

[43] Brown, W.E., DuRaine, G.D., Hu, J.C., Athanasiou, K.A. (2019). Structure-function relationships of fetal ovine articular cartilage. *Acta Biomaterialia*, vol. 87, p. 235-244, **DOI:10.1016/j.actbio.2019.01.073**.

[44] Su, W., Chen, H., Luo, Z. (2008). Effect of cyclic stretching on the tensile properties of patellar tendon and medial collateral ligament in rat. *Clinical Biomechanics*, vol. 23, no. 7, p. 911-917, **DOI:10.1016/j.clinbiomech.2008.04.002**.

[45] Suzuki, T., Mahfuz, H. (2018). Fatigue characterization of GFRP and composite sandwich panels under random ocean current loadings. *International Journal of Fatigue*, vol. 111, p. 124-133, **DOI:10.1016/j.ijfatigue.2018.02.004**.

[46] Hadidi, P., Cissell, D.D., Hu, J.C., Athanasiou, K.A. (2017). Temporal development of near-native functional properties and correlations with qMRI in self-assembling fibrocartilage treated with exogenous lysyl oxidase homolog 2. *Acta Biomaterialia*, vol. 64, p. 29-40, **DOI:10.1016/j.actbio.2017.09.035**.

[47] Hollis, L.O., Turner, R.E. (2018). The tensile root strength of five emergent coastal macrophytes. *Aquatic Botany*, vol. 146, p. 39-47, **DOI:10.1016/j.aquabot.2018.01.004**.

[48] Belyansky, I., Tsirline, B.V., Martin, T.R., Klima, D.A., Heath, J., Lincourt, A.E., Satishkumar, R., Vertegel, A., Heniford, B.T. (2011). The Addition of Lysostaphin Dramatically Improves Survival, Protects Porcine Biomesh from Infection, and Improves Graft Tensile Shear Strength. *Journal of Surgical Research*, vol. 171, no. 2, p. 409-415, **DOI:10.1016/j.jss.2011.04.014**.

[49] Iwasaki, H., Higashi, K., Nieh, T.G. (2004). Tensile deformation and microstructure of a nanocrystalline Ni–W alloy produced by electrodeposition. *Scripta Materialia*, vol. 50, no. 3, p. 395-399, **DOI:10.1016/j.scriptamat.2003.09.056**.

[50] Reicheneder, C.A., Gedrange, T., Lange, A., Baumert, U., Proff, P. (2009). Shear and tensile bond strength comparison of various contemporary orthodontic adhesive systems: An in-vitro study. *American Journal of Orthodontics and Dentofacial Orthopedics*, vol. 135, no. 4, p. 422.e1-422.e6, **DOI:10.1016/j.ajodo.2008.07.013**.

[51] Datta, D., Halder, G. (2018). Enhancing degradability of plastic waste by dispersing starch into low density polyethylene matrix. *Process Safety and Environmental Protection*, vol. 114, p. 143-152, **DOI:10.1016/j.psep.2017.12.017**.

[52] Wang, R., Liu, P., Cui, B., Kang, X., Yu, B. (2019). Effects of different treatment methods on properties of potato starch-lauric acid complex and potato starch-based films. *International Journal of Biological Macromolecules*, vol. 124, p. 34-40, **DOI:10.1016/j.ijbiomac.2018.11.207**.

[53] Younis, H.G.R., Zhao, G. (2019). Physicochemical properties of the edible films from the blends of high methoxyl apple pectin and chitosan. *International Journal of Biological Macromolecules*, vol. 131, p. 1057-1066, **DOI:10.1016/j.ijbiomac.2019.03.096**.

[54] Zhang, R., Wang, W., Zhang, H., Dai, Y., Dong, H., Hou, H. (2019). Effects of hydrophobic agents on the physicochemical properties of edible agar/maltodextrin films. *Food Hydrocolloids*, vol. 88, p. 283-290, **DOI:10.1016/j.foodhyd.2018.10.008**.

[55] Xiao, S., Gao, R., Gao, L., Li, J. (2016). Poly(vinyl alcohol) films reinforced with nanofibrillated cellulose (NFC) isolated from corn husk by high intensity ultrasonication. *Carbohydrate Polymers*, vol. 136, p. 1027-1034, **DOI:10.1016/j.carbpol.2015.09.115**.

[56] Liu, P., Kang, X., Cui, B., Wang, R., Wu, Z. (2019). Effects of glycerides with different molecular structures on the properties of maize starch and its film forming capacity. *Industrial Crops and Products*, vol. 129, p. 512-517, **DOI:10.1016/j.indcrop.2018.12.039**.

[57] Bosch Rexroth standard aluminum framing system, from https://www.boschrexroth.com/en/xc/products/product-groups/assembly-technology/topics/aluminum-profiles-solutions-components/aluminum-profiles-products/index, accessed on 2019-07-11.

[58] Berger Lahr stepper motor, from https://www.schneider-electric.com/en/download/document/0098441113309/, accessed on 2019-07-11.

[59] Bosch Rexroth linear compact module, from https://www.boschrexroth.com/en/us/products/product-groups/goto-products/goto-linear-motion/ckk-and-ckr-compact-modules/index, accessed on 2019-07-11.

[60] Schneider electric gearbox, from https://www.schneider-electric.com/en/product/GBX080003K/gearbox-straight-teeth-gbx---%C3%B8-80-mm---reduction-3%3A1-%3C-7-arc.min---85-n.m/, accessed on 2019-07-11.

[61] Berger Lahr motion control stepper motor drive, from https://www.schneider-electric.com/en/product/SD326RU68S2/motion-control-stepper-motor-drive---sd326---pulse-direction---%3C%3D-6.8-a/, accessed on 2019-07-11.

[62] AEP transducers tensile-compression load cell, from http://www.aeptransducers.com/load-cells/82-ts.html, accessed on 2019-07-11.

[63] AEP transducers analogue transmitter, from http://www.aeptransducers.com/instruments/164-ta4-2.html, accessed on 2019-07-11.

[64] Elgo magnetic linear encoder, from https://www.elgo.de/en/products/measuring-systems/linear-measurement-incremental/emix23/, accessed on 2019-07-11.

[65] Stojanović, A., Omerović, S., Krašna, S., Prebil, I. (2012). Mechanical properties of human cervical spine ligaments: Age related changes. *Journal of Biomechanics*, vol. 45, no. 1, p. S611, **DOI:10.1016/S0021-9290(12)70612-7**.

[66] National instruments motion controller NI PCI-7324, from http://www.ni.com/pdf/manuals/322503b.pdf, accessed on 2019-07-11.

[67] National instruments USB multifunction I/O device NI USB-6221, from http://www.ni.com/sl-si/support/model.usb-6221.html, accessed on 2019-07-11.

[68] Power over net HAT, from https://www.raspberrypi.org/products/poe-hat/, accessed on 2019-07-11.

[69] Raspberry Pi 3 B+ specifications, from https://static.raspberrypi.org/files/product-briefs/Raspberry-Pi-Model-Bplus-Product-Brief.pdf, accessed on 2019-07-11.

[70] Efftek ADC Baart board, from https://www.raspberrypi.org/forums/viewtopic.php?f=93&t=132508&p=883282&hilit=adc+board#p883282, accessed on 2019-07-11.

[71] Microchip Technology MCP 3208, from https://www.microchip.com/wwwproducts/en/MCP3208, accessed on 2019-07-11.

[72] Raspberry Pi GPIO overview, from https://www.raspberrypi.org/documentation/hardware/raspberrypi/gpio/README.md, accessed on 2019-07-11.

[73] Electrical specifications of GPIO pins on Raspberry Pi, from https://raspberrypi.stackexchange.com/questions/60218/what-are-the-electrical-specifications-of-gpio-pins/60219#60219, accessed on 2019-07-11.

[74] Microchip technology MCP6002, from https://www.microchip.com/wwwproducts/en/MCP6002, accessed on 2019-07-11.

[75] Mean Well 24V AC/DC power supply, from http://www.meanwellusa.com/webapp/product/search.aspx?prod=IRM-60, accessed on 2019-07-11.

[76] Mean Well 5V AC/DC power supply, from http://www.meanwellusa.com/webapp/product/search.aspx?prod=IRM-30, accessed on 2019-07-11.

[77] Controlling equipment source code "trgalnik", FSKMTM GitHub repository, from https://github.com/FSKMTM/trgalnik, accessed on 2019-10-28.

[78] National Instruments Multifunction modules – shop, from http://www.ni.com/en-us/shop/select/multifunction-io-category#facet:&productBeginIndex:0&orderBy:&pageView:grid&pageSize:&, accessed on 2019-07-11.

[79] Raspbian Stretch Lite: Version: April 2019 Release date: 2019-04-08), from https://www.raspberrypi.org/downloads/raspbian/, accessed on 2019-07-11.
[80] Real Time kernel 4.14.y-RT, from https://github.com/raspberrypi/linux/tree/rpi-4.14.y-rt, accessed on 2019-07-11.
[81] Pigpio library, from http://abyz.me.uk/rpi/pigpio/, accessed on 2019-07-11.
[82] Instron 8802 Fatigue testing system, from https://www.instron.us/en-us/products/testing-systems/dynamic-and-fatigue-systems/servohydraulic-fatigue/8802, accessed on 2019-07-11.

6 APPENDIX

Supplementary material consisting of measurement results, protocol, data saving and processing description, source code and connection scheme of the whole system is available at our GitHub repository: https://github.com/FSKMTM/trgalnik